Three-Dimensional Nitrogen-Doped Graphene Nanoribbons Aerogel as a Highly Efficient Catalyst for the Oxygen Reduction Reaction

Liang Chen, Ran Du, Jinghan Zhu, Yueyuan Mao, Cheng Xue, Na Zhang, Yanglong Hou, Jin Zhang, and Tao Yi**

Efficient catalysts for the cathodic oxygen reduction reaction (ORR) play a crucial role in the development of fuel cell technology.[1] Platinum-based materials have long been used as active catalysts for the ORR. However, due to the high cost, sluggish ORR process, susceptibility to methanol crossover, and limited stability of the platinum-based catalysts,[1] great efforts have been devoted to search for more efficient, durable, and inexpensive alternative ORR catalysts by employing non-precious metals (Fe, Co, etc.),[2] metal oxides (Fe_2O_3, Co_3O_4, $MnCo_2O_4$, etc.),[3] as well as metal-free heteroatom-doped carbon nanomaterials (porous carbon, carbon nanotubes, graphene, etc.).[4] Among them, carbon nanotubes (CNTs) and graphene-based materials have outperformed many of their counterparts in the past decades because of their unique features, including their high thermal conductivity, giant electron mobility, large surface area, and excellent stability.[5,6] As a rising star of the emerging carbon family, graphene nanoribbons (GNRs) have recently inspired a large amount of research in materials science for various applications in the fields of catalysis and nanoscale devices due to their unique structure and properties.[7,8] Compared to graphene nanosheets, which have irregular sizes and shapes, GNRs not only retain the unique characteristics of graphene sheets, such as their light weight, large surface area, and good conductivity, but they also possess special properties, such as a high length-to-width ratio, straight edges, and ideal surface regularity with few defects on the basal plane. These features make them more suitable for functional materials than random graphene sheets.[9] On the other hand, unlike graphene sheets that feature a zero bandgap, GNRs possess an open bandgap that varies with the ribbon width.[10] Moreover, chemical doping of GNRs with heteroatoms, such as N and B, can effectively realize further modulation of the electronic energy gap, thus enhancing the reactivity and electrocatalytic ability of the materials when used as ORR catalysts.[10]

Developing new graphene-based catalysts with good ORR performance not just in alkaline but also in acidic environments is desired because most fuel cells operate in acidic electrolytes. However, to the best of our knowledge, most graphene-based materials exhibit a good ORR activity in alkaline electrolytes, but poor activity in acids due to the relatively few catalytic sites formed within the materials.[11–15] To conquer the aforementioned drawbacks of these materials and acquire high-performance catalysts for fuel cells, a possible approach is to introduce a large number of active sites onto the graphene sheets without destroying their conjugated structures. However, conventional graphene-based materials are generally prepared by reduction from their oxidated precursor, namely graphene oxide (GO), which tends to lose its structural integrity and high electrical conductivity, a crucial property for electron transfer during electrocatalysis, because of the harsh oxidation and exfoliation.[11] Reduction through chemical and thermal approaches removes most of the oxygen-containing groups, but the defects usually remain, which inevitably breaks the regularity of the resulting reduced graphene samples.[16] Therefore, acquiring novel graphene-based catalysts with structural integrity as well as abundant active sites still remains a great challenge. GNRs prepared by longitudinally unzipping multi-walled carbon nanotubes do cater for these requirements. Assembling these GNRs into macroscopic bulk materials with desired structures and performances is one of the most powerful strategies for expanding the structural features of GNRs and creating novel physicochemical properties that differ from those of the individual components, thus, enriching the practical applications of GNRs. The assembly of GNRs into macroscopic aerogels, materials with an advanced three-dimensional (3D)

L. Chen, Y. Mao, C. Xue, Prof. T. Yi
Department of Chemistry and Concerted
Innovation Center of Chemistry for Energy Materials
Fudan University
220 Handan Road, Shanghai 200433, P.R. China
E-mail: yitao@fudan.edu.cn

R. Du, N. Zhang, Prof. J. Zhang
Center for Nanochemistry
Beijing National Laboratory for Molecular Sciences
Key Laboratory for the Physics and Chemistry of Nanodevices
State Key Laboratory for Structural
Chemistry of Unstable and Stable Species
College of Chemistry and Molecular Engineering
Peking University
Beijing 100871, P.R. China
E-mail: jinzhang@pku.edu.cn

J. Zhu, Prof. Y. Hou
Department of Materials Science and Engineering
College of Engineering
Peking University
Beijing 100871, P.R. China

DOI: 10.1002/smll.201402472

www.MaterialsViews.com

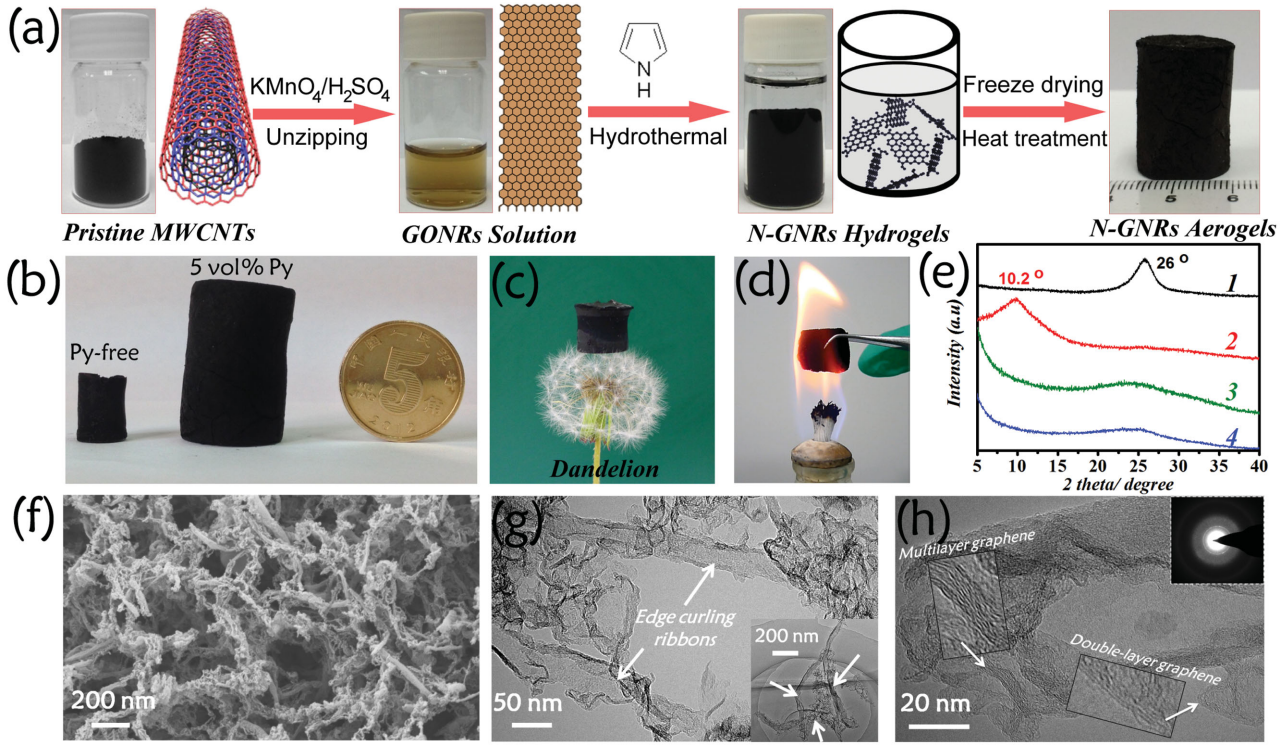

Figure 1. a) Illustration of the synthetic route for N-GNRs-A. b) Photographs of as-prepared 3D graphene nanoribbons aerogels derived from Py-free (left) and 5 vol% Py-containing (middle) GONRs suspension (10 mg mL^{-1}) after hydrothermal treatment. c) A monolith of ultralight N-GNRs-A standing on a dandelion. d) Photograph of N-GNRs-A in a hot flame of an alcohol burner. e) XRD patterns of 1) pristine MWCNTs, 2) GONRs, 3) GNRs-A, and 4) N-GNRs-A. f) SEM image of the resulting N-GNRs-A. g,h) Typical TEM and high-resolution TEM images of the as-prepared N-GNRs-A. Inset in (g) shows three interwoven curly nanoribbons. Inset in (h) is the selected-area electron diffraction (SAED) pattern of the aerogel.

architecture,[17] can not only integrate the intriguing properties of GNRs but also endow the material with the special features of aerogels. However, to the best of our knowledge, the assembly of GNRs into macroscopic 3D aerogels in a controlled manner coupled with doping of the gels with heteroatoms has not been explored.

In the present study, we have fabricated a highly conductive, ultralight, neat and versatile nitrogen-doped GNRs aerogel (denoted as N-GNRs-A) through a facile hydrothermal method for the first time. The N-GNRs-A possesses a very low density (2.5–22 mg cm^{-3}), large surface area (480–617 m^2 g^{-1}), and excellent conductivity (0.5–35.6 S m^{-1}) that depend on the initial concentration of the graphene oxide nanoribbons (GONRs). These properties allow the resultant aerogel to be used as an ORR electrocatalyst with a quite positive onset potential, high cathodic current density, and excellent durability, which are comparable or better than those of commercial Pt/C catalysts in alkaline medium. More interestingly, the N-GNRs-A catalyst also shows pronounced ORR electrocatalytic activity under acidic conditions.

Several approaches have been developed to prepare high-quality GNRs, including gas-phase oxidization,[18] lithographic,[19] sonochemical,[20] chemical vapor deposition[21] techniques as well as longitudinally unzipping multi-walled carbon nanotubes.[7] Among these approaches, only the last one can be utilized to prepare GNRs with a defined structure on a large scale. Thus, this approach was used to prepare the homogeneous GONRs in the present work. The experimental details are provided in the Supporting Information. For the preparation of ultralight, versatile N-GNRs-A, GONRs prepared by longitudinally unzipping multi-walled carbon nanotubes at a certain concentration (1–10 mg mL^{-1}) were mixed with 5 vol% pyrrole (Py) monomer. Hydrothermal treatment of the mixture at 180 °C for 12 h resulted in a mechanically robust monolithic hydrogel,[22–24] which was then freeze-dried and annealed at 1030 °C for 2 h under Ar atmosphere (see **Figure 1**a). Here, with a π-conjugated structure containing an electron-rich N atom, Py acts as the N source as it can be easily adsorbed onto the surface of the GONRs through hydrogen bonding and π–π interactions during the hydrothermal process. As a result, N atoms can be in-situ doped into the lattice of GNRs in the following high-temperature pyrolysis procedure. Moreover, the Py adsorbed on the GONRs can also act as a swelling agent or inhibitor to restrain the aggregation of GNRs in the process of gel formation.[12] Therefore, the amount of Py monomer is an important determinant of the character and quality of the gel. A low content of Py (<5 vol%) causes a certain shrinkage in the gel, whereas superfluous Py significantly increases the density of the gel. Using 5 vol% of the Py monomer, almost no shrinkage of the hydrogel occurs. Figure 1b indicates that, compared to the Py-free pure GNRs aerogel (denoted as GNRs-A), the N-GNRs-A possessed an obviously larger volume, leading to a quite low density (2.5 ± 0.5 mg cm^{-3}) when the initial concentration of GONRs was 1 mg mL^{-1}. This value was slightly higher than some of the carbon-based aerogels (0.16–2.1 mg cm^{-3}),[12,25,26] but much lower than that of other 3D carbon-based architectures

small NANO MICRO

(Table S1 in the Supporting Information).[27–31] The ultralight aerogel can be placed on top of a dandelion without breaking it (Figure 1c). Furthermore, the aerogel is thermostable and fire-resistant. A piece of N-GNRs-A emits red light on an alcohol burner instead of catching fire, possibly because of the quick removal of heat during combustion because of its high porosity (Figure 1d). Thermogravimetric analysis (TGA) curves indicate that the as-prepared N-GNRs-A shows a weight loss of about 2.6 wt% at a temperature of up to 800 °C in N_2 and it can bear a temperature of approximately 400 °C in air without significant weight loss (Figure S1, Supporting Information).

The structure and morphology of the as-prepared N-GNRs-A samples were investigated by X-ray diffraction (XRD) (Figure 1e), Raman spectroscopy (Figure S2, Supporting Information), scanning electron microscopy (SEM) (Figure 1f), and transmission electron microscopy (TEM) (Figure 1g,h). The XRD pattern clearly confirmed the longitudinal unzipping of the multi-walled carbon nanotubes (MWCNTs) to GONRs and the subsequent formation of the GNRs aerogel.[7] Generally, it can be seen from Figure 1e that the pristine MWCNTs have a broad peak at 26°, which corresponds to the (002) reflection of the carbon nanotubes. Upon unzipping, the obtained GONRs shared a broad peak at 10.2° corresponding to the (001) reflection, which is very similar to that of GO,[17] indicating that the interlayer space of the GONRs was much larger than that of the pristine MWCNTs due to the unzipping process and further introduction of oxygen-containing functional groups into the GNRs. Following the hydrothermal procedure and heat treatment, a broad peak located at approximately 26° reappeared in the spectrum for the N-GNRs-A. To further verify the above results, UV-visible spectra, SEM, and TEM images of the pristine MWCNTs and as-obtained GONRs are also provided in the Supporting Information. The pristine CNTs exhibit a strong absorption peak at 248 nm that can be ascribed to $\pi \rightarrow \pi^*$ transitions of the aromatic C-C bonds. After unzipping, the absorption of the resulting GONRs blue-shifted from 245 to 229 nm (Figure S3, Supporting Information), similar to that when peeling off GO, further confirming the complete unzipping of the CNTs to GONRs. The SEM images show that the N-GNRs-A exhibits an interconnected, porous structure with hierarchical pores ranging from hundreds of nanometers to tens of micrometers (Figure S4, Supporting Information). A similar morphology can also be observed in the SEM images of Py-free GNRs-A and N-doped aerogel before pyrolysis (Figure S5, Supporting Information). Moreover, the TEM images further indicated that the three-dimensional structure of the aerogel was constructed by ribbon-like sheets, namely GNRs (marked by the arrows in Figure 1g). High-resolution TEM revealed that these ribbon-like walls typically consist of double layers or multilayers of graphene sheets (Figure 1h). However, because of the strong oxidation effect, which inevitably gives rise to imperfections in the product precursor (GONRs), the as-prepared nanoribbons show a slightly narrow and curly morphology, as can be seen from the SEM and high-resolution TEM (HRTEM). Similar morphologies and interpretations have been published before.[7,10]

X-ray photoelectron spectroscopy (XPS) was used to analyze the chemical attributes of N-GNRs-A and GONRs (**Figure 2**a and Figure S6, Supporting Information). As expected, the XPS spectrum of the GONRs showed only C and O peaks, whereas additional N peaks were observed for the N-GNRs-A, which confirmed the doping of N atoms within the aerogel (2.8%, N/C atomic ratio). The significant decrease in O content from 32.3% for the GONRs to 2.07% for the N-GNRs-A can be attributed to the reduction of the GONRs during the high-temperature pyrolysis process, which was further affirmed by comparing the high-resolution C 1s spectra of the two samples (Figure S7, Supporting Information). The high-resolution N 1s spectrum of N-GNRs-A reveals the presence of both pyridinic (398.5 eV) and pyrrolic (401 eV) N atoms (Figure 2b), indicating that the N atoms have been doped into the lattice of the GNRs.[32] Brunauer–Emmett–Teller (BET) analysis showed that the specific surface area of N-GNRs-A can reach up to 617 $m^2\ g^{-1}$ (Figure 2c), which is much larger than that of previously reported graphene-based aerogels (270–280 $m^2\ g^{-1}$),[12,25] GNR or GNR–CNT hybrid aerogels obtained by in-situ chemical unzipping (113 $m^2\ g^{-1}$)[28] and other 3D carbon-based frameworks,[12,18,27–36] suggesting large open pores within the aerogel, which is consistent with the SEM observations. The surface areas of both N-GNRs-A and GNRs-A are much higher than that of the precursors GONRs (31 $m^2\ g^{-1}$, Figure S8 and S9, Supporting Information), indicating that the porous structure of N-GNRs-A mainly comes from the hydrothermal assembly process. The specific surface area of N-GNRs-A was further confirmed by using a standard methylene-blue absorption method (Figure S10, Supporting Information). The values obtained via this method are slightly higher than that of the BET values, which may be caused by the fact that methylene-blue absorption measures not only the mesopores but also the macropores within the aerogels, whereas the nitrogen adsorption–desorption test can only measure the mesopores. Despite its porous structure, the resulting N-doped aerogel also possessed a high conductivity of up to 35.6 S m^{-1} (Movie S1, Supporting Information, and Figure 2d), which is much higher than (or comparable to) those of pure graphene aerogels and other graphene-based materials, as has been reported previously.[24,37] The high conductivity of N-GNRs-A facilitates electron transfer through the entire material to the surface of the electrode and guarantees a high electrocatalytic activity for ORR, as described below.

GNRs, a kind of 1D carbon material derived from carbon nanotubes,[6,7] can serve as an ideal bridge combining the features of CNTs and graphene sheets. The one-atom thick GNRs with quasi-one-dimensional (1D) planar geometry does not only provide a large specific surface area but also facilitates electron transport, and hence it can be more effective than CNTs and graphene sheets for catalysis. Inspired by the superb chemical and physical properties of the N-GNRs-A demonstrated above, we expected that the aerogel might have great potential for ORR catalysis. The ORR catalytic performance of N-GNRs-A (ρ = 22 mg cm^{-3}) was investigated using cyclic voltammetry (CV) in a N_2- and O_2-saturated 0.1 M aqueous KOH electrolyte solution at a scan rate

www.MaterialsViews.com

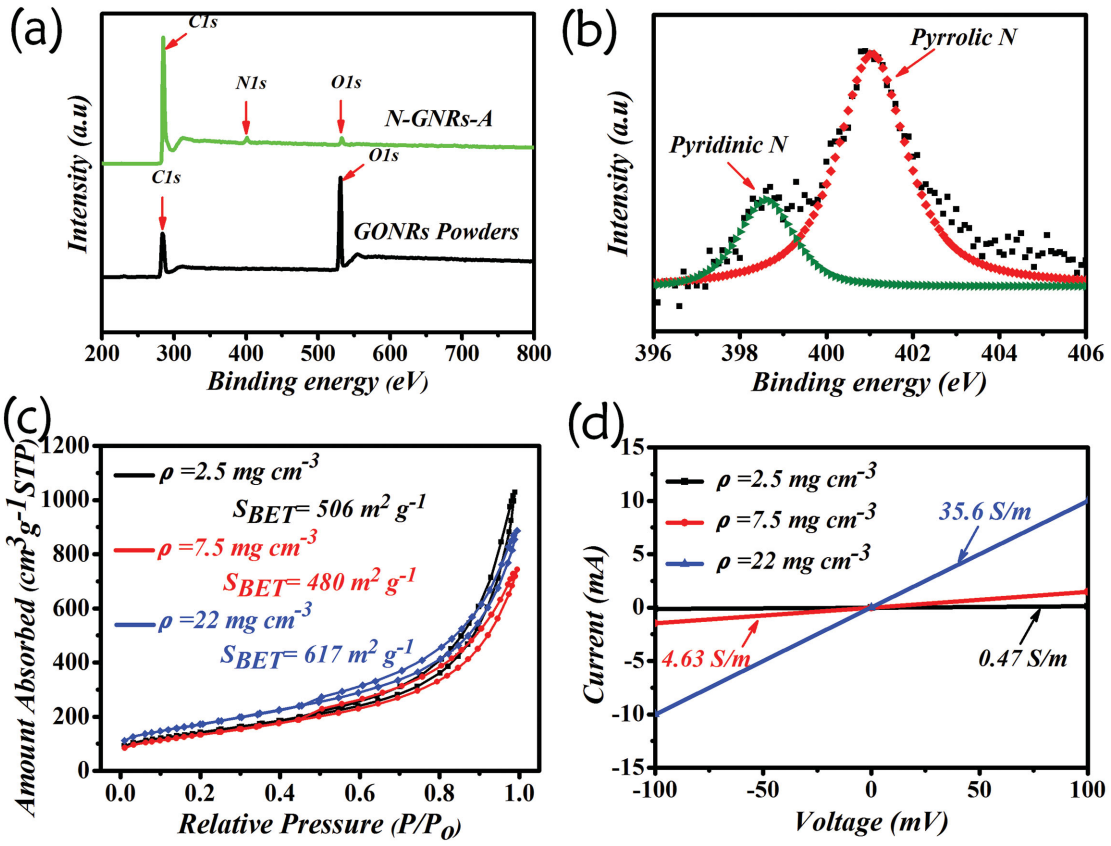

Figure 2. a) XPS survey profiles of the resulting GONRs powder and N-GNRs-A. b) High-resolution N 1s peak of as-prepared N-GNRs-A. c) Nitrogen sorption isotherms of as-obtained N-GNRs-A with different densities. d) Typical *I–V* curves of N-GNRs-A with different densities.

of 10 mV s^{-1} (**Figure 3**a). Unlike the Py-free GNRs aerogel, which has no obvious redox peak (Figure S11, Supporting Information), the N-GNRs-A exhibited a significant redox peak at approximately –0.19 V, representing the O_2 reduction process in O_2-saturated KOH solution.[38,39] For comparison, the related tests of N-GNRs-A catalysts with different mass loading are provided in the Supporting Information (Figure S12,S13). The results show that with an increase in mass loading of catalyst per area the onset potential of the catalyst does not change significantly, however, the cathodic current density presents a marked increase. To gain additional insight into the role of N-GNRs-A in the ORR, linear sweep voltammetry (LSV) curves were recorded on a rotating ring-disk electrode (RRDE) in an O_2-saturated 0.1 M KOH solution at a scan rate of 10 mV s^{-1} (Figure 3b). The N-GNRs-A sample has a high onset potential of around –0.05 V, which is only 0.08 V more negative than that of a Pt/C electrode (20 wt% Pt on carbon black has an onset potential of ca. 0.03 V), but much more positive than that of GNRs-A and MWCNTs (<–0.15 V, Figure 3b). This onset potential is also much more positive than that of most heteroatom-doped graphene-based materials and typical porous carbon-based materials (Table S2, Supporting Information).[12,13,15] Moreover, the ORR kinetic current density of the N-GNRs-A is also much higher than other reference catalysts. The more positive onset potential as well as the higher current density of N-GNRs-A may be attributed to the perfect synergistic effect of the doped pyridinic and pyrrolic N species as well as the interconnected porous structure, large specific surface area, and good conductivity. Thus, oxygen could be easily adsorbed onto the catalyst surface with preferred configuration in a large quantity, and the electrons required for ORR could be transferred into the catalyst without difficulty.

It is well known that conventional electrocatalysts generally possess sluggish ORR kinetics and often suffer from poor electron transfer to the adsorbed oxygen molecules, which generally results in the occurrence of a two-electron reduction of oxygen as well as the desired four-electron reduction. The two-electron process is less favorable because of its lower efficiency and the corrosive nature of the resulting hydrogen peroxide (H_2O_2). To further confirm the electron transfer number (n) and the H_2O_2 yield of N-GNRs-A during the ORR process, RRDE curve of N-GNRs-A at 1600 rpm were performed as shown in Figure 3c. The n values of the N-GNRs-A electrode at different potentials were calculated to be 3.71–3.96. Moreover, the measured H_2O_2 yield on the N-GNRs-A electrode was found to be less than 14.7% over the entire potential range (Figure 3d and Figure S14, Supporting Information), which is similar to that of the recently reported N,S-codoped graphene nanomesh (N-S-GMF) and other heteroatom-doped carbon-based materials,[14,15] further confirming the one-step, 4-electron ORR process of the N-GNRs-A electrode. The RDE measurements as well as the corresponding K–L plots also confirmed the efficient 4-electron dominated ORR process (Figure 3e-f, Figure S15, Supporting Information).

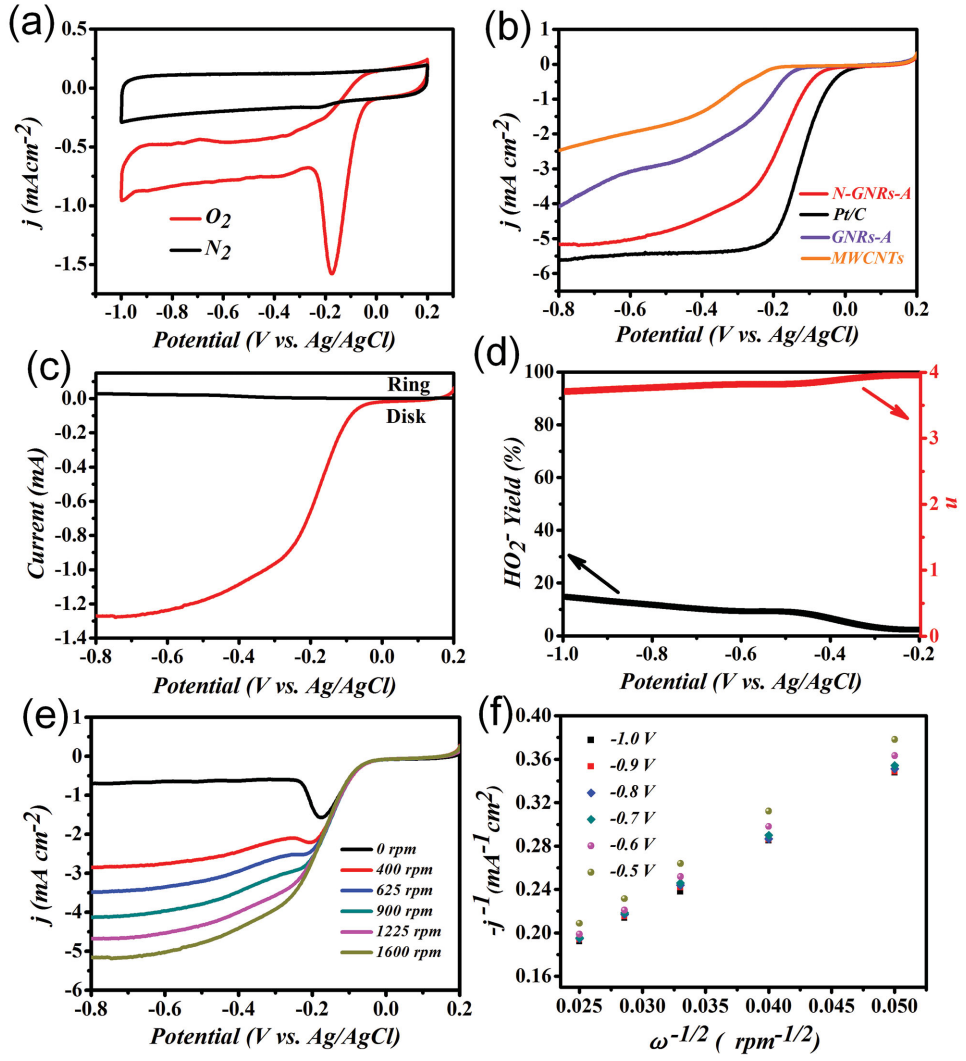

Figure 3. The ORR performance for N-GNRs-A in alkaline solution. a) CV curves of N-GNRs-A in a N_2 - and O_2 -saturated 0.1 M KOH solution at a scan rate of 10 mV s^{-1}. b) LSV curves of pristine MWCNTs, GNRs-A, N-GNRs-A, and Pt/C in an O_2 -saturated 0.1 M KOH solution at a scan rate of 10 mV s^{-1} and a rotation speed of 1600 rpm. c) RRDE curves of N-GNRs-A at 1600 rpm. d) Peroxide percentage and electron transfer number (n) of N-GNRs-A within the potential range of –1.0 V to –0.2 V. e) RDE curves of N-GNRs-A in an O_2-saturated 0.1 M KOH solution with various rotation speeds at a scan rate of 10 mV s^{-1}. f) K–L plots of J^{-1} vs. $\omega^{-1/2}$ at different electrode potentials derived from RDE measurements (with mass loading of 0.08 mg cm^{-2})

In light of practical applications in fuel cells it is well known that fuel molecules (e.g., methanol) may pass through the membrane from anode to cathode and poison the cathode catalyst. The N-GNRs-A electrode was therefore subjected to further testing with regards to the crossover effect and its long-term stability for the ORR. **Figure 4**a shows the current–time (i–t) chronoamperometric responses for the ORR at N-GNRs-A and Pt/C electrodes. After adding 3 M methanol to the electrolyte an obvious inversion of the current density was observed for the Pt/C electrode, whereas the N-GNRs-A electrode remained almost unchanged, suggesting the excellent tolerance of the N-GNRs-A electrode to methanol. Lastly, the durability of N-GNRs-A was also compared with that of a commercial Pt/C catalyst. Nearly 78% of the current density was retained after continuous work for 20 000 s for the N-GNRs-A electrode, which was similar to that of other heteroatom-doped graphene nanomaterials[15,29] but well higher than that of expensive Pt/C catalysts (approximately 60%) (Figure 4b), indicating that the N-GNRs-A electrocatalyst is much more stable than commercial Pt/C in an alkaline medium.

In addition, the electrocatalytic performance of N-GNRs-A for ORR in acidic medium was also investigated. The CV curve indicated a significant reduction process for N-GNRs-A with a pronounced cathodic ORR peak at 0.20 V versus Ag/AgCl electrode when the electrolyte (0.5 M H_2SO_4) was saturated with O_2 (Figure S16a, Supporting Information), whereas no obvious response was observed at the same potential range under N_2. To further quantify the ORR electron-transfer pathway, we employed an RRDE technique as shown in Figure S16b. The N-GNRs-A catalyst exhibited an ORR process approximating a 4-electron transfer pathway (n = 3.66–3.92 over the potential range of –0.2 V to 0.4 V, Figure S16c, Supporting Information) with a low H_2O_2 yield

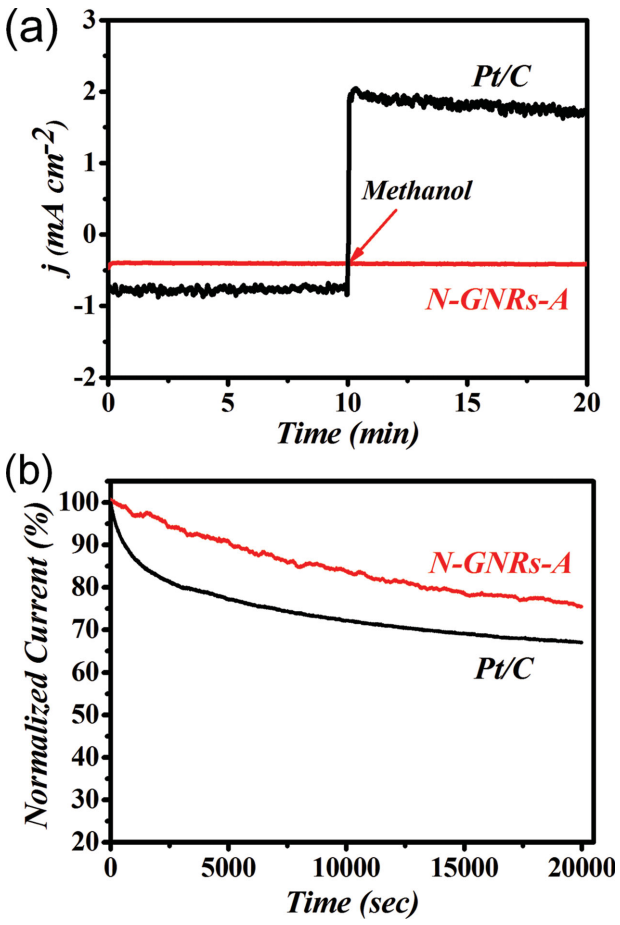

Figure 4. a) Methanol crossover effect on N-GNRs-A and Pt/C upon addition of 3 M methanol after about 10 min in an O_2-saturated 0.1 M KOH solution at –0.4 V. b) Current–time chronoamperometric response of N-GNRs-A and Pt/C catalysts at –0.4 V in O_2 saturated 0.1 M KOH aqueous solution at a rotation rate of 1600 rpm.

of 4.2–17.1% over the measured potential range. These results are similar to that of the recently reported N-S-GMF[14] and nitrogen-doped carbon nanosheets (NDCNs),[15] but is still inferior to previously reported work.[40,41] The LSV curves of the N-GNRs-A at different electrode rotation speeds also confirmed the above RRDE results (Figure S16d, Supporting Information).

The excellent electrocatalytic performance of N-GNRs-A for the ORR both in alkaline and acidic solutions may be derived from the unique 1D regular structure of GNR that differs from random graphene sheets. The conventional precursors of graphene (namely, graphene oxide) always lose their structural integrity and high electrical conductivity, whereas GNRs prepared by longitudinally unzipping of multi-walled carbon nanotubes can preserve their structural integrity and high electrical conductivity as well as endow extra catalytic sites to the electrode by incorporating oxygen-containing functional groups during the unzipping process. Additionally, Py serves as a swelling agent to suppress the shrinking of the gel. As a result, the as-prepared aerogel possesses a large amount of pores in the 3D gel network, thus insuring the efficient mass transfer to the active sites and markedly facilitating the ORR diffusion kinetics. The doped N species further enhances the reactivity and electrocatalytic ability of the GNRs.[11–15] Moreover, aerogels with large surface areas can inevitably lead to more efficient access to the electrolyte compared to other doped powder or film counterparts. The good conductivity of N-GNRs-A also plays a vital role in the ORR by facilitating the electron transfer between the N-GNRs-A and oxygen. All of the results mentioned above support the conclusion that N-GNRs-A is an efficient catalyst for ORR both in alkaline and acidic solutions.

In summary, a highly conductive, ultralight, neat and versatile nitrogen-doped GNRs aerogel has been fabricated via a facile hydrothermal method and exhibits an ultra-low density, large surface area, and good conductivity. The obtained aerogel can act as a novel ORR catalyst with superb electrocatalytic activity and better stability than commercial Pt/C catalysts in alkaline medium. Interestingly, the N-GNRs-A electrode also has a remarkable ORR performance in acidic solutions. Its excellent catalytic properties for ORR may be attributed to the perfect synergistic effect of the N-doped, structural integrity of the GNRs, its nanoporous structure, high surface area, and good conductivity. We believe that the ORR performance of the GNRs-based materials can be further optimized by introducing other heteroatoms or realizing co-doping with atoms such as B, P, and S. Our future work will focus on this direction. The aerogel presented here may open up a significant avenue for the fabrication of a series of high-performance GNR-based porous materials with promising applications.

Experimental Section

experimental details see the Supporting Information.

Supporting Information

Supporting Information is available from the Wiley Online Library or from the author.

Acknowledgements

The authors acknowledge the financial support from the National Basic Research Program of China (2013CB733700), the China National Funds for Distinguished Young Scientists (21125104), the National Natural Science Foundation of China (51373039), the Specialized Research Fund for the Doctoral Program of Higher Education (20120071130008), the Program for Innovative Research Team in University (IRT1117), the Program of Shanghai Subject Chief Scientist (12XD1405900), and the Shanghai Leading Academic Discipline Project (B108). We also thank Chenyu Xu and Prof. Liangti Qu from the Beijing Institute of Technology for the RRDE tests.

[1] B. C. Steele, A. Heinzel, *Nature* **2001**, *414*, 345.
[2] D. S. Su, G. Q. Sun, *Angew. Chem. Int. Ed.* **2011**, *50*, 11570.
[3] Y. Y. Liang, Y. G. Li, H. L. Wang, J. G. Zhou, J. Wang, T. Regier, H. J. Dai, *Nat. Mater.* **2011**, *10*, 780.

[4] S. Wang, I. Eswaramoorthi, A. Roy, Y. Xue, D. Yu, L. M. Dai, *Angew. Chem. Int. Ed.* **2011**, *50*, 11756.
[5] S. Iijima, *Nature* **1991**, *354*, 56.
[6] A. K. Geim, K. S. Novoselov, *Nat. Mater.* **2007**, *6*, 183.
[7] D. V. Kosynkin, A. L. Higginbotham, A. Sinitskii, J. R. Lomeda, A. Dimiev, B. K. Price, J. M. Tour, *Nature* **2009**, *458*, 872.
[8] M. A. Rafiee, W. Lu, A. V. Thomas, A. Zandiatashbar, J. Rafiee, J. M. Tour, N. A. Koratkar, *ACS Nano* **2010**, *4*, 7415.
[9] A. L. Higginbotham, D. V. Kosynkin, A. Sinitskii, Z. Z. Sun, J. M. Tour, *ACS Nano* **2010**, *4*, 2059.
[10] L. Chen, Y. Hernandez, X. L. Feng, K. Müllen, *Angew. Chem. Int. Ed.* **2012**, *51*, 7640.
[11] Y. Li, W. Zhou, H. Wang, L. Xie, Y. Liang, F. Wei, J. C. Idrobo, S. J. Pennycook, H. J. Dai, *Nat. Nanotechnol.* **2012**, *7*, 394.
[12] Y. Zhao, C. Hu, Y. Hu, H. Cheng, G. Shi, L. Qu, *Angew. Chem. Int. Ed.* **2012**, *51*, 11 371.
[13] J. Liang, Y. Jiao, M. Jaroniec, S. Z. Qiao, *Angew. Chem. Int. Ed.* **2012**, *51*, 11 496.
[14] Y. Zhao, C. Hu, L. Song, L. Wang, G. Q. Shi, L. M. Dai, L. T. Qu, *Energy Environ. Sci.* **2014**, *7*, 1913.
[15] W. Wei, H. Liang, K. Parvez, X. Zhuang, X. L. Feng, K. Müllen, *Angew. Chem. Int. Ed.* **2014**, *53*, 1570.
[16] D. Zhou, Y. Cui, P. W. Xiao, M. Y. Jiang, B. H. Han, *Nat. Commun.* **2014**, doi: 10.1038/ncomms5716.
[17] L. Chen, B. Wei, X. Zhang, C. Li, *Small* **2013**, *9*, 2331.
[18] L. Jiao, X. Wang, G. Diankov, H. Wang, H. Dai, *Nat. Nanotechnol.* **2010**, *5*, 321.
[19] L. Tapaszto, G. Dobrik, P. Lambin, L. P. Biro, *Nat. Nanotechnol.* **2008**, *3*, 397.
[20] X. Li, X. Wang, L. Zhang, S. Lee, H. Dai, *Science* **2008**, *319*, 1229.
[21] J. Campos-Delgado, J. M. Romo-Herrera, X. Jia, D. A. Cullen, H. Muramatsu, Y. A. Kim, T. Hayashi, Z. Ren, D. J. Smith, Y. Okuno, T. Ohba, H. Kanoh, K. Kaneko, M. Endo, H. Terrones, M. S. Dresselhaus, M. Terrones, *Nano Lett.* **2008**, *8*, 2773.
[22] Y. Li, J. Chen, L. Huang, C. Li, J. D. Hong, G. Q. Shi, *Adv. Mater.* **2014**, DOI: 10.1002/adma.201400657.
[23] C. Li, G. Q. Shi, *Adv. Mater.* **2014**, *26*, 3992.
[24] Y. Xu, K. Sheng, C. Li, G. Q. Shi, *ACS Nano* **2010**, *4*, 4324.
[25] H. Y. Sun, Z. Xu, C. Gao, *Adv. Mater.* **2013**, *25*, 2554.
[26] M. Mecklenburg, A. Schuchardt, Y. K. Mishra, S. Kaps, R. Adelung, A. Lotnyk, L. Kienle, K. Schulte, *Adv. Mater.* **2012**, *24*, 3486.
[27] H. W. Liang, Q. F. Guan, L. F. Chen, Z. Zhu, W. J. Zhang, S. H. Yu, *Angew. Chem. Int. Ed.* **2012**, *51*, 5101.
[28] Q. Peng, Y. Li, X. He, X. Gui, Y. Shang, C. Wang, C. Wang, W. Zhao, S. Du, E. Shi, P. Li, D. H. Wu, A. Y. Cao, *Adv. Mater.* **2014**, *26*, 3241.
[29] Z. S. Wu, S. B. Yang, Y. Sun, K. Parvez, X. L. Feng, K. Müllen, *J. Am. Chem. Soc.* **2012**, *134*, 9082.
[30] H. Hu, Z. Zhao, W. Wan, Y. Gogotsi, J. Qiu, *Adv. Mater.* **2013**, *25*, 2219.
[31] Z. H. Tang, S. L. Shen, J. Zhuang, X. Wang, *Angew. Chem. Int. Ed.* **2010**, *49*, 4603.
[32] Z. J. Fan, J. Yan, L. J. Zhi, Q. Zhang, T. Wei, J. Feng, M. Zhang, W. Z. Qian, F. Wei, *Adv. Mater.* **2010**, *22*, 3723.
[33] M. A. Worsley, P. J. Pauzauskie, T. Y. Olson, J. Biener, J. H. Satcher Jr., T. F. Baumann, *J. Am. Chem. Soc.* **2010**, *132*, 14067.
[34] Y. Xu, Z. Lin, X. Huang, Y. Liu, Y. Huang, X. F. Duan, *ACS Nano* **2013**, *6*, 656.
[35] S. Nardecchia, D. Carriazo, M. L. Ferrer, M. C. Gutiérrez, F. Monte, *Chem. Soc. Rev.* **2013**, *42*, 794.
[36] Z. S. Wu, A. Winter, L. Chen, Y. Sun, A. Turchanin, X. L. Feng, K. Müllen, *Adv. Mater.* **2012**, *24*, 5130.
[37] X. Zhang, Z. Sui, B. Xu, S. Yue, Y. Luo, W. Zhan, B. Liu, *J. Mater. Chem.* **2011**, *21*, 6494.
[38] C. Zhang, N. Mahmood, H. Yin, F. Liu, Y. Hou, *Adv. Mater.* **2013**, *25*, 4932.
[39] L. Wang, A. Ambrosi, M. Pumera, *Angew. Chem. Int. Ed.* **2013**, *52*, 13 818.
[40] W. Ding, Z. Wei, S. Chen, X. Qi, T. Yang, J. Hu, D. Wang, L. J. Wan, S. F. Alvi, L. Li, *Angew. Chem. Int. Ed.* **2013**, *52*, 11 755.
[41] X. Wang, J. S. Lee, Q. Zhu, J. Liu, Y. Wang, S. Dai, *Chem. Mater.* **2010**, *22*, 2178.

Received: August 18, 2014
Revised: September 15, 2014
Published online: November 3, 2014